Colorimetric Microneedle Patches for Multiplexed Transdermal Detection of Metabolites

Dan Dan Zhu[1], Le Wen Zheng[1], Phan Khanh Duong[1], Reanne Hui Cheah[1], Xin Yi Liu[1], Jun Ren Wong[2], Wen Jun Wang[3], Steven Thng Tien Guan[4], Xin Ting Zheng[5] and Peng Chen[1,4,6]**

[1]School of Chemical and Biomedical Engineering, Nanyang Technological University, 637457, Singapore.

[2]Singapore Institute of Technology, 138683, Singapore

[3]School of Physical Science and Information Technology, Liaocheng University, Liaocheng 252059, PR China

[4]Skin Research Institute of Singapore, 308232, Singapore.

[5]Institute of Materials Research and Engineering, Agency for Science, Technology and Research (A*STAR), 138634, Singapore.

[6]Lee Kong Chian School of Medicine, Institute for Digital Molecular Analytics and Science, Nanyang Technological University, 636921, Singapore.

*Corresponding author. Email: zhengxt@imre.a-star.edu.sg; chenpeng@ntu.edu.sg

Abstract

Skin Interstitial Fluid (ISF) is an alternative source for biomarkers. Herein, a highly swellable microneedle patch (MNP) to rapidly extract ISF painlessly and bloodlessly is presented. The MNP is made of crosslinked methacrylated hyaluronic acid (MeHA) and dissolvable hyaluronic acid (HA) with the optimal balance of mechanical strength (0.6 N/MN) and absorption capability (16.22 μL in 20 minutes). Incorporated with wax-patterned and sensing-reagent-decorated test paper (TP) for multiplexed colorimetric detection of metabolites (glucose, lactate, cholesterol, and pH), this TP-MNP biosensor gives rapid color change in biomarker concentration-dependent manner based on specific enzymatic reactions, whereby allowing diagnosis by the naked eye or quantitative RGB analysis. Both the *in vitro* and *in vivo* experiments demonstrate the feasibility of TP-MNPs to detect multiple biomarkers in skin interstitial fluid within minutes. Such convenient and self-administrable profiling of metabolites shall be instrumental for home-based long-term monitoring and management of metabolic diseases.

Keywords: microneedles, metabolites, skin interstitial fluid, transdermal detection

Introduction

Chronic diseases demand constant monitoring of relevant biomarkers in order to optimize the treatment based on condition changes (Chen et al. 2019; Hong and Lee 2019; Kukkar et al. 2022). But this is difficult because biomarker detection conventionally relies on invasive blood sampling and tedious laboratory procedures (Silva et al. 2018). To solve the problem, non-invasive sensors have been developed to detect biomarkers from sweat, tears, saliva, and urine (Alwan et al. 2010; Gandhi and Pinney 2014; Mujeeb-U-Rahman et al. 2019). However, biomarkers present in these biofluids are limited and have poor correlation with their presence in blood in terms of concentration and dynamics, therefore often offering low diagnostic value (Mohan et al. 2020; Sanati et al. 2022).

Interstitial fluid (ISF) in skin tissue formed by blood transcapillary filtration is an attractive source of biomarkers because 79% of its components are common with plasma and it has some unique biomarkers specific for some diseases (e.g., melanoma) (Shi et al. 2020; Wang et al. 2020). But because of the stratum corneum barrier, the metabolites in ISF can hardly permeate to the skin surface for readily detection (Ullah et al. 2018). Hence, suction blister technique is used to extract ISF for analysis, which can only be conducted in clinics by skilled professionals and cause discomfort even infection (Niedzwiecki et al. 2018). Microneedles (MNs) that can minimal-invasively penetrate skin stratum corneum to extract ISF through capillary force or vacuum suction have been devised (Cárcamo-Martínez et al. 2021; Nicholas et al. 2018; Than et al. 2020; Wang et al. 2005). Alternatively, swellable polymeric MNs have been demonstrated for ISF absorption (Yadav et al. 2022). Although microneedle patches (MNPs) can be easily administrated, these reported methods require a long sampling time and extra devices for operation and analysis (Donnelly et al. 2014). For example, MNs made of poly(methylvinylether-co-maelic anhydride) take 1 hour to extract ~0.84 mg ISF (Hong et al. 2014; Romanyuk et al. 2014). Methacrylated hyaluronic acid (MeHA) (Chang et al. 2017; Zheng et al. 2020) and polyvinyl alcohol (PVA) (Samant et al. 2020) based MNs with better swellability have been demonstrated. In these studies, centrifugation was used to recover the adsorbed ISF and laboratory apparatuses were needed for off-line analysis. In a recent work, an antibody-coated polystyrene MNPs was devised to capture protein biomarkers in ISF for off-line enzyme-linked immunosorbent assay with much enhanced sensitivity (Wang et al. 2021). But the functionalization of MNs and the need of a microplate reader for fluoroimmunoassay complicates the procedure. For point-of-care diagnosis, efforts have been recently made to incorporate enzymes and dye molecules into MNs for colorimetric detection of glucose (Shen et al. 2021) and uric acid (He et al. 2021). However, leak of sensing reagents and by-products produced by the enzymatic reactions from MNPs into skin is of major concern (Joel et al. 2014; Saravanakumar et al. 2017). Although it has been shown that conjugating glucose oxidase (GOD) on nanoparticles in MNP-based colorimetric glucose sensors prevent escape of the enzyme into skin tissue, leak of dye

molecules and H_2O_2 is not avoided and further complexity for MNP preparation is introduced (Hsu et al. 2020; Wang et al. 2020).

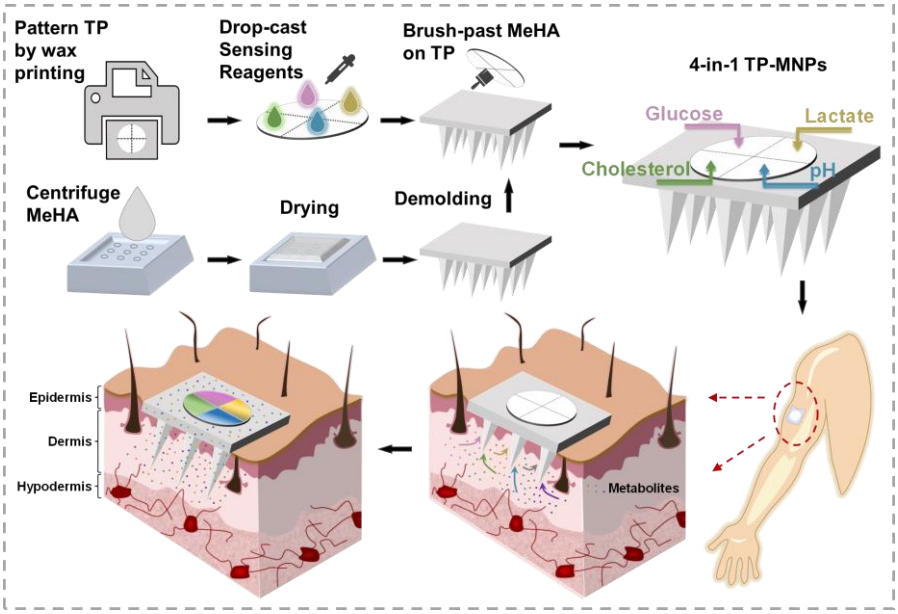

Figure 1. Schematic illustration of the fabrication and application process of test-paper incorporated microneedle patches (TP-MNPs).

To tackle the aforementioned issues, we herein demonstrate colorimetric MNPs for multiplexed transdermal detection of metabolites (Figure 1). MNs are made of crosslinked MeHA and dissolvable osmolytes, which are rapidly and highly swellable with good mechanical strength. Test papers (TPs), which are wax-patterned and functionalized with enzymes and dye molecules, are incorporated with MNPs to colorimetrically report the concentrations of glucose, cholesterol, lactate, and pH in ISF. This approach provides opportunities for long-term monitoring and optimized management of chronic diseases by enabling self-administrable constant profiling of biomarkers in ISF, which is amenable for convenient home-based use with good patient compliance.

Methods

Materials: Sodium hyaluronic acid (HA, Mw 200-400 kDa) was purchased from Freda Biochem Co., Ltd. (China). Methacrylic anhydride (MA, 94%, 276685), N,N-Dimethylformamide (DMF, 227056) and cobalt(II) chloride hexahydrate ($CoCl_2 \cdot 6H_2O$)

were supplied by Sigma (USA). Glucose, sodium L-lactate, cholesterol, bromocresol green dye, horseradish peroxidase (HRP), glucose oxidase (GOD), lactate oxidase (LOD), cholesterol oxidase (COD), 4-aminoantipyrine (4-AAP), o-phenylenediamine (OPD), 2,2′-Azino-bis(3-ethylbenzthiazoline-6-sulfonic acid) (ABTS), Stabilicoat® Immunoassay Stabilizer solution and sodium 3,5-dichloro-2-hydroxybenzenesulfonate (DHBS) were obtained from Merck. Nitrocellulose membrane was purchased from Bio-Rad (USA).

Fabrication of Microneedle Patches (MNPs): To synthesize methacrylate modified hyaluronic acid (MeHA), 4g HA was first dissolved in 200 mL deionized (DI) water in the ice bath, followed by the addition of 133.3 mL N,N-Dimethylformamide (DMF). Then, 4.76 mL methacrylic anhydride (MA) was dropwise added into the mixture and stirred for 4 hours with pH being maintained at 8-9. The reaction was kept at 4°C overnight with continuous stirring. Subsequently, 9.88 g NaCl was added to the solution, and after ethanol precipitation, MeHA was obtained and purified in a dialysis tube with DI water for 7 days. Finally, purified MeHA was lyophilized and stored at 4°C for further usage.

To fabricate microneedles, MeHA solution (50 mg/mL in DI water) with photo-initiator (Irgacure 2959, 0.5 mg/mL) was prepared without or with cellulose, sucrose, or hyaluronic acid (HA) (weight ratio to MeHA of 1:1). The mixed solution was cast into a 10 × 10 polydimethylsiloxane (PDMS, Dow Corning 184 Sylgard) mold, centrifuged at 4000 rpm for 5 minutes, then naturally dried overnight in a dry cabinet.

Fabrication of Test Paper Embedded Microneedle Patches (TP-MNPs): A nitrocellulose membrane (0.2 μm pore–size) was chosen as the host substrate for sensing reagents including chromogenic dyes, horseradish peroxidase (HRP) and oxidases. Wax patterns were printed onto the nitrocellulose membrane to create hydrophobic boundaries whereby defining distinct detection regions by a wax printer (Xerox® ColorQube® 8580 Color Printer). The wax-printed nitrocellulose membrane was then heated at 90 °C for 4 minutes to ensure sufficient penetration of wax barriers into the nitrocellulose membrane, thus preventing undesirable mixing of different

sensing reagents between the detection quadrants.

The sensing reagents for glucose included 8 mM 4-AAP in DHBS buffer, 0.3 mg/mL HRP and 10 mg/mL glucose oxidase (GOD) in DI water. The sensing reagents for lactate included 10 mM OPD, 0.15 mg/mL HRP and 5 mg/mL lactate oxidase (LOD) in DI water. The sensing reagents for cholesterol included 10 mM ABTS, 0.15 mg/mL HRP and 1 mg/mL cholesterol oxidase (COD) in DI water. The sensing reagent for pH is 0.04 wt% bromocresol green in DI water. For glucose, lactate and cholesterol detection, quadrants were firstly modified with 0.5 mL chitosan solution (1mg/mL in 0.2% acetic acid). After drying, 0.5 μL of chromogenic dye solution, HRP solution, and respective oxidases were uniformly drop-cast onto the respective sensing quadrants on the nitrocellulose membrane, followed by another addition of 0.5 μL dye solution. To prepare the pH sensing quadrant, 0.5 μL bromocresol green solution (0.04 wt%) was drop-casted twice and then air-dried. The nitrocellulose membrane was cut out into pieces with a size just smaller than that of a MNP, and brush-painted with a thin layer of MeHA solution as the liquid adhesive and then pasted onto the microneedle substrate. After drying, the integrated TP-MNPs were exposed to UV light (wavelength = 360 nm, intensity = 17.0 mW/ cm^2, model 30, OAI) for 300 seconds to crosslink MeHA. To avoid MN softening due to ambient humidity and the possible problems caused by dye oxidation or enzyme degradation, MNPs were kept in a sealed hermetic bag at 4 ℃ before use.

Characterization of Microneedle Patches: The mechanical property of the microneedles was characterized by a tensile compression machine (MTS C42, USA). Specifically, MNPs were fixed on the flat stainless-steel platen with a vertical force applied against the needle tips at a speed of 0.1 mm/min. The morphology of the microneedles before and after swelling was revealed by scanning electron microscopy (SEM, Hitachi TM 4000 Plus).

To investigate the water absorption rate, TPs coated with cobalt chloride ($CoCl_2$) were prepared. Specifically, 5 g of hydrated cobalt(II) chloride was dissolved in 100 mL DI water and the nitrocellulose membrane was then soaked in this solution for 10 minutes,

and dried in an oven (at 80 °C). The $CoCl_2$ TP was sealed onto the MNP using a waterproof adhesive plaster to avoid damp. To examine the swelling, water absorption rate, and sensing performance, TP-MNPs were applied onto a parafilm-covered 4 wt% agarose hydrogel (skin mimic) and observed under an optical microscope (Leica DM6). Agarose hydrogels were prepared to contain defined concentrations of glucose (0-16 mM), lactate (0-3.2 mM), cholesterol (0-12 mM) or proton (pH 5.0-8.0). Optical images of the TP-MNPs after being applied onto agarose gels were analyzed by the RGB Histogram plugin in ImageJ. Statistical analysis was performed using Student's t-test for two-group comparison (GraphPad Prism 7).

Detection of Metabolites In Vivo: The performance of MNPs incorporated with glucose-sensing TPs was evaluated on mice (male C57BL/6JInv, age 8 wk). TP-MNPs were applied onto the back of hair-shaved mice for 10 minutes and then removed for imaging and analysis. Then the mice were intraperitoneally injected with glucose solution at a concentration of 2 g kg^{-1} in 200 μL PBS, followed by glucose detection after 30 minutes. Subsequently, insulin (2 U kg^{-1} in 200 μL PBS) was injected, which was followed by glucose detection 30 minutes later. The blood glucose level of mice was also simultaneously measured from tail vein blood using a multi-monitoring meter (BeneCheck, China) for comparison. MNPs incorporated with 4-in-1 patterned TPs were also employed to simultaneously assess glucose, lactate, cholesterol and pH in both mouse skin and human skin.

Results and Discussion

For colorimetric analysis of extracted interstitial fluid, microneedles (MNs) should be non-dissolvable yet highly swellable, and have sufficient mechanical strength for skin penetration as well as high water affinity to allow rapid and significant absorption of ISF. In addition, microneedles and the supporting substrate should be highly transparent. Here cross-linked methacrylate-modified hyaluronic acid (MeHA) was adopted as the matrix material for MNP. MeHA MNP has been widely used for ISF extraction (Chen et al. 2020). Hyaluronic acid (HA) is a biocompatible polymer existing in our connective tissues and is often used to make dissolvable MNs for transdermal drug

delivery (Zan et al. 2019). Non-dissolvable MeHA-MNs are not as hard as HA-MNs and their absorption rate is not fast enough to ensure sufficient permeation of ISF into the substrate in minutes. Hoping for improvement, soluble osmolytes (cellulose, sucrose, or HA) were blended into the MeHA matrix.

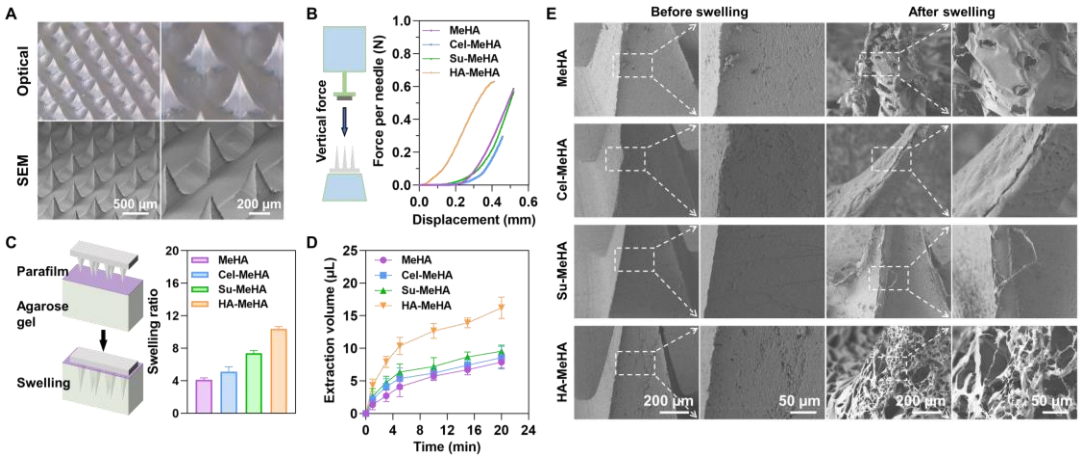

Figure 2. Characterization of microneedles. A) Optical and scanning electron microscopy (SEM) images of crosslinked MeHA MNPs. B) Mechanical properties of MeHA-MNs without or with the addition of osmolytes (cellulose – Cel, sucrose – Su, or hyaluronic acid – HA; weight ratio to MeHA of 1:1). C) Swelling ratios of different MeHA MNPs (10 × 10 array, n = 6 per group) after being applied onto a parafilm-covered agarose gel for 20 minutes. D) The liquid extraction volume from agarose gel by the MNPs. E) SEM images of the MNPs before and after swelling.

MNPs were fabricated using a simple micro-molding method (Figure 1), as previously reported (Than et al. 2017; Than et al. 2018). Aiming to enhance the ISF-adsorption ability of MNs, dissolvable osmolytes (cellulose, sucrose, or hyaluronic acid) with the weight ratio to MeHA of 1:1 was added to MeHA solution. On the other hand, too much osmolytes would lead to disintegration of MNs upon insertion into skin, which is not desirable for ISF extraction. Both optical and scanning electron microscopy (Figure 2A) show that the MNs (600 μm long) exhibit a pyramidal structure with a sharp tip (~10 μm). The insertion force of 0.1 N/MN is required to pierce into skin. As shown in Figure 2B, all types of MNPs have sufficient mechanical strength for skin penetration. Among the three osmolytes, only HA greatly enhanced the mechanical strength of the

microneedles. Specifically, HA-MeHA MN can exert 0.6 N/needle for easy skin penetration.

Agarose gel (4% agar + 96% phosphate buffer solution to mimic ISF) covered with a water-impermeable parafilm (mimicking stratum corneum) was used as the artificial skin model to investigate the ability of MNPs to extract ISF. Applying an HA-MeHA MNP equipped with an array of 10 × 10 MNs onto it for 20 minutes led to a significant mass increase (10.37 times) due to fluid absorption through MNs (Figure 2C), outperforming MeHA MNP (4.12 times), Cel-MeHA MNPs (5.13 times) and Su-MeHA MNP (7.37 times). Having an exponential absorption kinetics with a time constant of 20 min (Figure 2D), ~16.22 μL of fluid was drawn into HA-MeHA MNP, outperforming MeHA MNP (7.89 μL), Cel-MeHA MNPs (8.57 μL) and Su-MeHA MNP (9.55 μL). As revealed by SEM (Figure 2E), despite of significant swelling, the morphology of the four types of microneedles was well preserved. But HA-MeHA MNs became highly porous presumably because HA could easily dissolve away, accounting for the superior absorption ability of such MN.

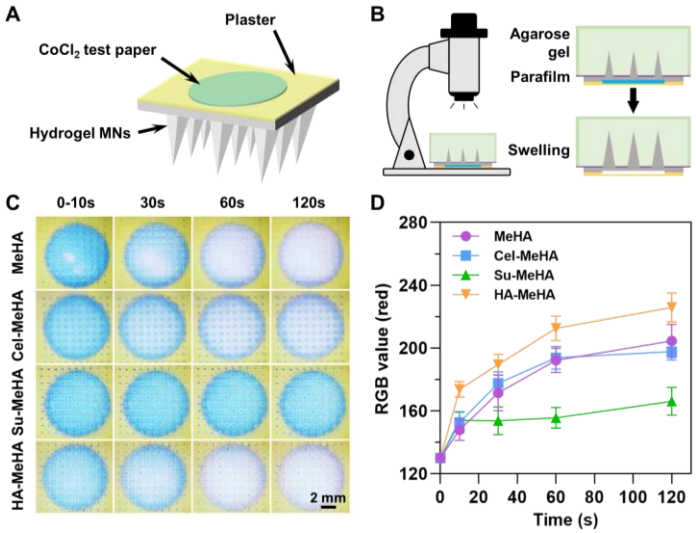

Figure 3. A) Schematic of $CoCl_2$ TP-MNPs. B) Schematic of the water absorption rate study on $CoCl_2$ TP-MNPs by using parafilm-covered agarose gel to mimic skin model. C) Images of $CoCl_2$ TP-MNPs after insertion into parafilm-agar and the color changing in 120 seconds. D) Quantitive analysis of the color changes from the images in (C) by the RGB Histogram plugin in ImageJ.

To examine the absorption rate, a nitrocellulose membrane (test paper) imbued with $CoCl_2$ salt ($CoCl_2$ TP) was placed on the backside of MNP and sealed with a water-proof adhesive plaster (Figure 3A). $CoCl_2 \cdot 6H_2O$ is a commonly used compound to quickly measure the presence of water by the readily color change from blue (dehydration) to pale pink (hydration). $CoCl_2$ TP-MNPs were applied onto the agarose skin model and observed under an optical microscope (Figure 3B). As demonstrated in Figure 3C and 3D, TP in HA-MeHA MN was fully sopped within 2 minutes with a wetting time constant of 120 s. The absorption rate of HA-MeHA MNP was the fastest as compared with other MNPs. Taken together, the addition of HA largely enhanced the mechanical strength, swelling-ability, and absorption rate of MeHA MNP. Addition of cellulose or sucrose increased swelling-ability to a certain extent whereas sucrose compromised absorption rate. Therefore, in the following experiments, HA-MeHA MNPs were used.

As demonstrated above, HA-MeHA MNPs shall be able to penetrate into skin and effectively extract ISF whereby enabling colorimetric detection based on reactions between the biomarkers in ISF with the reagents immobilized on the embedded TP. Profiling the metabolites in ISF is instrumental for the diagnosis and management of metabolic diseases such as diabetes, obesity, and cardiovascular disease. As the proof-of-concept demonstration, four typical chronical disease-related biomarkers, including glucose, lactate, cholesterol and pH, were chosen as the targets. We drop-casted TPs with chromogenic dye 4-aminoantipyrine (4-AAP) together with glucose oxidase (GOD) and horseradish peroxidase (HRP) for glucose sensing, or chromogenic dye o-phenylenediamine (OPD) together with lactate oxidase (LOD) and HRP for lactate sensing, or chromogenic dye 2,2′-Azino-bis(3-ethylbenzthiazoline-6-sulfonic acid) (ABTS) together with cholesterol oxidase (COD) and HRP for cholesterol sensing, respectively. Upon oxidation of the metabolite specifically catalysed by its respective oxidase, hydrogen peroxide (H_2O_2) is produced. Subsequently, HRP reduces H_2O_2 into hydroxyl radicals, which in turn reduces the chromogenic dye into its colored form. As for pH sensing, in acidic aqueous solution (pH=3.8-5.4), bromocresol green is ionized

to the monoanionic form (yellow); and at higher pH, it is deprotonated to a dianionic form (blue). The paper-based sensor was brush-painted with a thin layer of MeHA solution as the liquid adhesive and glued onto the microneedle substrate. Subsequently, the TP-MNP was completely dried and crosslinked under UV for 5 minutes.

For healthy individuals, the normal blood glucose value ranges from 3.9 to 6.1 mM at fasting, and may reach up to 7.9 mM in 2 hours after a meal. For diabetic patients, the plasma glucose exceeds 7.0 mM with an empty stomach or 11.1 mM with a 2-hour post-prandial test. Timely monitoring of the varying blood glucose level is the key to optimized management of diabetes. But the conventional finger pricking blood test is not practical for frequent application due to poor patient compliance. The painless and bloodless microneedle approach offers an alternative. Firstly, based on the agarose skin model containing defined glucose concentrations and an application duration of 5 minutes, we demonstrated that the glucose-sensing TP-MNPs could visually report the glucose concentration in ISF ranging from 0 to 16 mM (Figure 4A). Wetting of the TP was not perfectly uniform presumably due to the heterogeneity of microneedle structure and penetration. Therefore, for all the experiments, we chose an area of 1.0 × 1.5 mm (2 × 3 microneedles underneath) with the deepest color change for analysis. The representative images of the color changes on glucose TPs resulting from hypoglycemia (light purple) to hyperglycemia (deep purple) were presented in Figure 4A. The color change was quantified by RGB histogram analysis. When dye 4-AAP turned purple in a glucose-dependent manner, the values of all three channels decreased in similar trends. As the green channel showed the steepest change, the maximum RGB value (255) minus the green RGB value was used to positively correlate with the glucose level. The average response curve from several measurements (3-5 times) shown in Figure 4A was employed to infer the glucose concentrations in *in vivo* experiments. Similar strategies were applied for the colorimetric detection of the other biomarkers.

Blood lactate level depends on oxygen supply and metabolism. It is a biomarker to indicate the severity of diseases such as acute carbon monoxide poisoning, sepsis, neonatal asphyxia, trauma, and acute hemorrhagic shock. Timely detection of lactate is

essential for monitoring patients in critical ills. Normal blood lactate concentration falls in the range of 0.5-1.7 mM at rest and modestly rises after exercise. Tissues and organs with high metabolic rates are most affected by hyperlactacidemia (> 2 mM), such as muscle weakness and hepatic failure. As seen in Figure 4B, the colorimetric analysis of OPD-coated TP based on green RGB value can linearly report lactate level up to 3.2 mM. Hyperlactacidemia as indicated by deep orange color can be easily recognized by naked eyes.

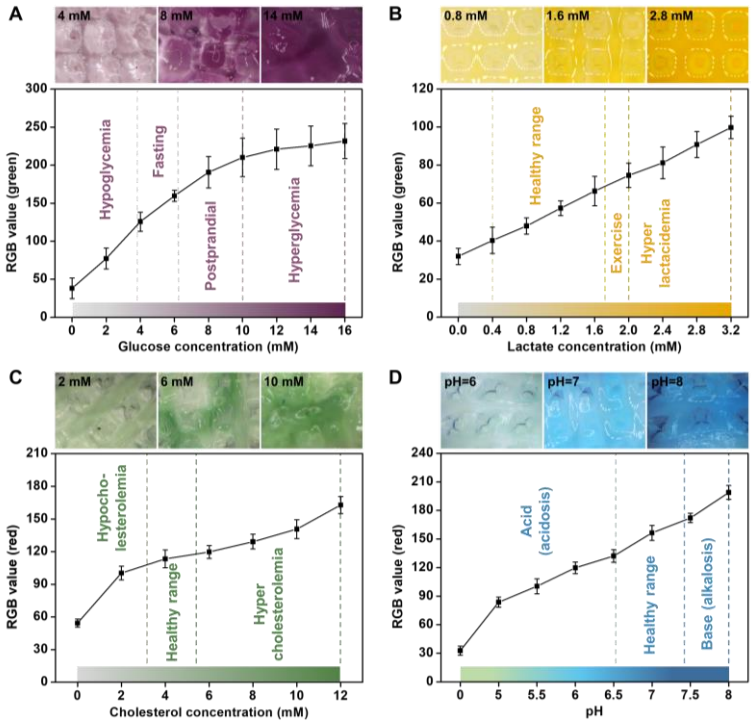

Figure 4. *In vitro* detections of the four biomarkers (i.e., glucose, lactate, cholesterol and pH) using agarose gel as the skin model. Images of HA-MeHA TP-MNPs after colorimetric detection of glucose (A), lactate (B), cholesterol (C) and pH (D) were recorded and analyzed using the RGB Histogram plugin in ImageJ.

Blood cholesterol level >5.72 mM increases the risk to develop kidney failure, stroke, and cardiovascular diseases. It is recommended by the Centers for Disease Control and Prevention (CDCP) of USA to check cholesterol level regularly because unmanaged cholesterol levels over the years might be challenging to treat. As shown in Figure 4C, the colorimetric analysis of ABTS-coated TP based on red RGB value can detect cholesterol level up to 12 mM. Hypercholesterolemia can be detected when TP turns

into thick green.

Blood pH level has to be precisely maintained between 7.35 – 7.45 to properly support metabolic reactions. Below this range, dizziness, drowsiness, anxiety, even mental confusion occurs. Beyond 7.45 causes muscle cramp and heart problems. As shown in Figure 4D, the colorimetric analysis of bromocresol green-coated TP based on red RGB value can report pH value ranging from 5 to 8. Greenish cyan color and navy blue indicate acidosis and alkalosis, respectively. The different physiological conditions indicated by the concentrations of these four metabolites can be distinguished by naked eyes based on colors or by quantitative statistical analyses (Figure S1).

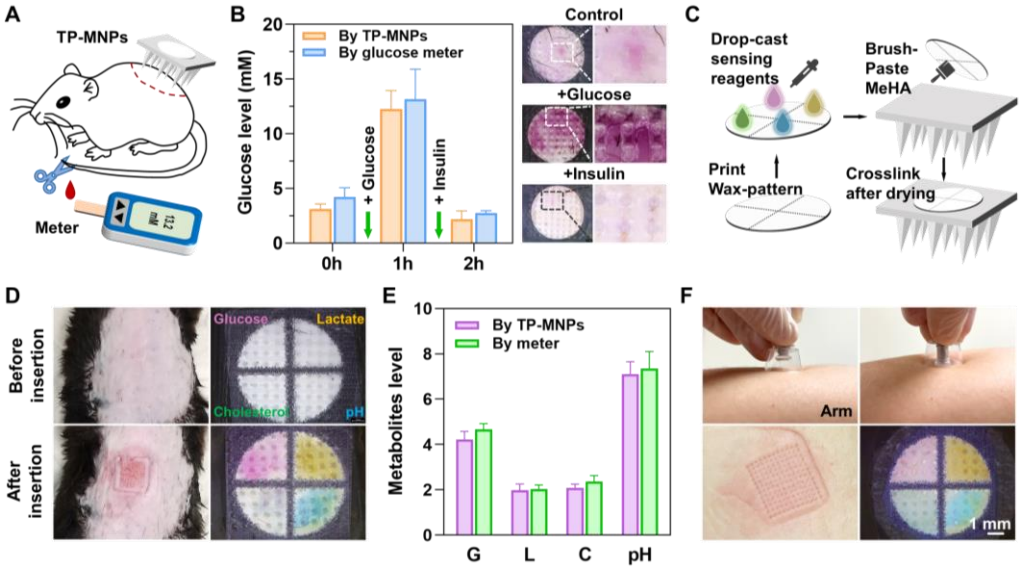

Figure 5. A) Schematic illustration of the animal experiment. Detection of metabolites in mice was conducted using TP-MNPs on hair-removed dorsal skin and a multi-monitoring meter via blood from the tail vein. B) Mouse was intraperitoneally injected with glucose (2 g kg^{-1}) and insulin (2 U kg^{-1}). The glucose level was detected in 30 minutes to avoid lag time. C) Schematic illustration of fabricating 4-in-1 TP-MNPs. D) 4-in-1 patterned TP-MNPs on mice back. E) The comparison of the glucose – G, lactate – L, cholesterol – C and pH levels inferred from TP-MNPs and detected with a commercial meter. (n = 5 mice per group). F) TP-MNPs were applied to human arms using a commercial applicator. Images of the skin and the TP-MNPs before and after insertion were taken.

The *in vivo* performance of TP-MNP was further investigated on mice and compared with the blood test using a commercial glucose meter (Figure 5A). As shown in Figure 5B, the glucose level in ISF determined by the color change after TP-MNP being pressed onto the mouse skin using a mechanical applicator for 10 min was ≈3.13 mM. And as expected, intraperitoneal injection of glucose (2g/kg) raised the level to ≈12.26 mM after 30 minutes while subsequent injection of insulin (2U/kg) brought down it to 2.17 mM after 30 minutes. The monitoring by the glucose meter reported the same trend. It also indicated that the glucose level in blood was slightly higher than that in ISF, consistent with the previous report (Heikenfeld et al. 2019). This is generally true for other metabolites as well because they are exuded through the blood vessels into ISF and reach an equilibrium with a certain time delay (García-Guzmán et al. 2021; Teymourian et al. 2021).

As metabolic disorders alter the profile of metabolites, simultaneous detection of multiple metabolites is desirable for accurate diagnosis and assessment (Li et al. 2020; Liu et al. 2019). Here, a 4-in-1 patterned TP was devised with four well-defined non-interfering quadrants (Figure 5C). Specifically, patterns of solid wax were printed using a wax-printing machine and melted by a hot plate to penetrate the full thickness of the nitrocellulose membrane, whereby creating complete hydrophobic barriers between different reaction zones. Then the sensing reagents for the four metabolites (glucose, cholesterol, lactate, pH) were drop-casted onto each quadrant. The 4-in-1 TP-MNPs were thumb-pressed on the shaved dorsal skin of mice for 10 minutes. The penetration points were visible on the skin and the 4-in-1 TP changed color after insertion (Figure 5D). The levels of glucose, lactate, cholesterol and pH inferred from image analysis were 4.22 mM, 1.98 mM, 2.09 mM and 7.11, respectively, which were slightly lower than the real-time value read by the multi-monitoring meter (for glucose, lactate and cholesterol, BeneCheck, China) and the pH meter (Laqua Horiba, Japan) in a legitimate and acceptable range (Figure 5E), as said above. Further, as a proof-of-concept demonstration, 4-in-1 TP-MNP was applied on the arm of one of the researchers using a commercial applicator (Micropoint Technologies). Ten minutes after being applied,

the MNPs were removed, leaving temporary marks on the skin and resulting in color changes on the TP (Figure 5F). The inferred glucose, lactate, cholesterol and pH levels were 3.69 mM, 1.92 mM, 2.13 mM and 7.08, respectively, all falling into the normal physiological range. Marks caused by MN insertion on both mouse and human skin disappear in 30 minutes without leaving any residues, dye molecules, redness or wound (Figure S2), suggesting the good biocompatibility of TP-MNPs. Our experiments demonstrated the feasibility of self-administrating TP-MNPs to profile metabolites for home-based long-term monitoring of metabolic diseases to enable personalized and optimized treatment.

Conclusion

In this study, we demonstrate that adding hyaluronic acid as the osmolyte greatly enhances the capacity and rate of the microneedles made of non-dissolvable crosslinked methacrylated hyaluronic acid to extract skin interstitial fluid, as well as their mechanical strength for easy skin penetration. The microneedle patch is incorporated with the test paper which is wax-patterned and decorated with sensing reagents for simultaneous colorimetric detection of multiple biomarkers in the extracted interstitial fluid (specifically glucose, lactate, cholesterol and pH). Its feasibility is demonstrated by *in vitro* experiments on an artificial skin model, *in vivo* mouse experiments, and a test on a human volunteer. The microneedle patch can be easily self-administrated and the detection can be evaluated by naked eyes. In principle, smartphones with specifically developed programs can be used for quantitative RGB analysis. Also, it is conceivable that other metabolites (e.g., uric acid) can be similarly assayed. And combining the interstitial fluid-extracting microneedle patch with colorimetric, fluorescence, electrical, or electrochemical sensors will allow the detection of a wide spectrum of biomarkers in interstitial fluid, promising the potential to change the landscape of medical practice for chronic diseases.

Acknowledgment

This research was financially supported by AcRF Tier-1 grants (RG110/20 and RT02/20)

and AcRF Tier-2 grant (MOE2019-T2-2-004) from Singapore Ministry of Education, and Mini-BEP grant (SC25/21-815116) from Agency of Science, Technology and Research (A*STAR) of Singapore.

References

Alwan, A., MacLean, D.R., Riley, L.M., d'Espaignet, E.T., Mathers, C.D., Stevens, G.A., Bettcher, D., 2010. The Lancet 376, 1861-1868.

Cárcamo-Martínez, Á., Mallon, B., Domínguez-Robles, J., Vora, L.K., Anjani, Q.K., Donnelly, R.F., 2021. Int. J. Pharm. 599, 120455.

Chang, H., Zheng, M., Yu, X., Than, A., Seeni, R.Z., Kang, R., Tian, J., Khanh, D.P., Liu, L., Chen, P., Xu, C., 2017. Adv. Mater. 29, 1702243.

Chen, X., Dong, T., Wei, X., Yang, Z., Matos Pires, N.M., Ren, J., Jiang, Z., 2019. Biosens. Bioelectron. 142, 111453.

Chen, Z., He, J., Qi, J., Zhu, Q., Wu, W., Lu, Y., 2020. Drug Discov. Today 25, 1462-1468.

Donnelly, R.F., Mooney, K., McCrudden, M.T.C., Vicente-Pérez, E.M., Belaid, L., González-Vázquez, P., McElnay, J.C., David Woolfson, A., 2014. J. Pharm. Sci. 103, 1478-1486.

Gandhi, P.U., Pinney, S., 2014. Ann. Glob. Health 80, 46-54.

García-Guzmán, J.J., Pérez-Ràfols, C., Cuartero, M., Crespo, G.A., 2021. TrAC, Trends Anal. Chem. 135, 116148.

He, R., Liu, H., Fang, T., Niu, Y., Zhang, H., Han, F., Gao, B., Li, F., Xu, F., 2021. Adv. Sci. 8, 2103030.

Heikenfeld, J., Jajack, A., Feldman, B., Granger, S.W., Gaitonde, S., Begtrup, G., Katchman, B.A., 2019. Nat. Biotechnol. 37, 407-419.

Hong, X., Wu, Z., Chen, L., Wu, F., Wei, L., Yuan, W., 2014. Nanomicro. Lett. 6, 191-199.

Hong, Y., Lee, S.H., 2019. Int. J. Nurs. Stud. 92, 1-15.

Hsu, W. L., Huang, C.-Y., Hsu, Y. P., Hwang, T. L., Chang, S. H., Wang, H. Y. J., Feng, L. Y., Tzou, S. J., Wei, K. C., Yang, H. W., 2020. Chem. Eng. J. 398, 125536.

Li, H., Lin, H., Lv, W., Gai, P., Li, F., 2020. Biosens. Bioelectron. 165, 112336.

Liu, X., Li, X., Gao, X., Ge, L., Sun, X., Li, F., 2019. ACS Appl. Mater. Interfaces 11, 15381-15388.

Joel, S., Turner, K.B., Daunert, S., 2014. ACS Chem. Biol. 9, 1595-1602.

Kukkar, D., Zhang, D., Jeon, B.H., Kim, K.-H., 2022. TrAC, Trends Anal. Chem. 150, 116570.

Mohan, A.M.V., Rajendran, V., Mishra, R.K., Jayaraman, M., 2020. TrAC, Trends Anal. Chem. 131, 116024.

Mujeeb-U-Rahman, M., Honarvar Nazari, M., Sencan, M., 2019. Biosens. Bioelectron. 124-125, 66-74.

Nicholas, D., Logan, K.A., Sheng, Y., Gao, J., Farrell, S., Dixon, D., Callan, B., McHale, A.P., Callan, J.F., 2018. Int. J. Pharm. 547, 244-249.

Niedzwiecki, M.M., Samant, P., Walker, D.I., Tran, V., Jones, D.P., Prausnitz, M.R., Miller, G.W., 2018. Anal. Chem. 90, 3786-3792.

Romanyuk, A.V., Zvezdin, V.N., Samant, P., Grenader, M.I., Zemlyanova, M., Prausnitz, M.R., 2014. Anal. Chem. 86, 10520-10523.

Samant, P.P., Niedzwiecki, M.M., Raviele, N., Tran, V., Mena-Lapaix, J., Walker, D.I., Felner, E.I., Jones, D.P., Miller, G.W., Prausnitz, M.R., 2020. Sci. Transl. Med. 12, eaaw0285.

Sanati, A., Esmaeili, Y., Bidram, E., Shariati, L., Rafienia, M., Mahshid, S., Parlak, O., 2022. Appl. Mater. Today 26, 101350.

Saravanakumar, G., Kim, J., Kim, W.J., 2017. Adv. Sci. 4, 1600124.

Shen, D., Yu, H., Wang, L., Chen, X., Feng, J., Li, C., Xiong, W., Zhang, Q., 2021. Eur. Polym. J. 148, 110348.

Shi, A., Kasumova, G.G., Michaud, W.A., Cintolo-Gonzalez, J., Díaz-Martínez, M., Ohmura, J., Mehta, A., Chien, I., Frederick, D.T., Cohen, S., Plana, D., Johnson, D., Flaherty, K.T., Sullivan, R.J., Kellis, M., Boland, G.M., 2020. Sci. Adv. 6, eabb3461.

Silva, T.E., Ronsoni, M.F., Schiavon, L.L., 2018. Diabetes. Metab. Syndr. 12, 431-440.

Teymourian, H., Tehrani, F., Mahato, K., Wang, J., 2021. Adv. Healthc. Mater. 10, 2002255.

Than, A., Liang, K., Xu, S., Sun, L., Duan, H., Xi, F., Xu, C., Chen, P., 2017. Small Methods 1, 1700269.

Than, A., Liu, C., Chang, H., Duong, P.K., Cheung, C.M.G., Xu, C., Wang, X., Chen, P., 2018. Nat. Commun. 9, 4433.

Than, A., Zan, P., Chen, P., 2020. VIEW 1, e21.

Ullah, S., Hamade, F., Bubniene, U., Engblom, J., Ramanavicius, A., Ramanaviciene, A., Ruzgas, T., 2018. Biosens. Bioelectron. 110, 175-179.

Wang, J., Wuethrich, A., Sina Abu Ali, I., Lane Rebecca, E., Lin Lynlee, L., Wang, Y., Cebon, J., Behren, A., 2020. Trau, M., Sci. Adv. 6, eaax3223.

Wang, P.M., Cornwell, M., Prausnitz, M.R., 2005. Diabetes Technol. Ther. 7, 131-141.

Wang, Z., Li, H., Wang, J., Chen, Z., Chen, G., Wen, D., Chan, A., Gu, Z., 2020. Biomaterials 237, 119782.

Wang, Z., Luan, J., Seth, A., Liu, L., You, M., Gupta, P., Rathi, P., Wang, Y., Cao, S., Jiang, Q., Zhang, X., Gupta, R., Zhou, Q., Morrissey, J.J., Scheller, E.L., Rudra, J.S., Singamaneni, S., 2021. Nat. Biomed. Eng. 5, 64-76.

Yadav, P.R., Dobson, L.J., Pattanayek, S.K., Das, D.B., 2022. Chem. Eng. Sci. 247, 117005.

Zan, P., Than, A., Duong, P.K., Song, J., Xu, C., Chen, P., 2019. Adv. Ther. 2, 1900064.

Zheng, M., Wang, Z., Chang, H., Wang, L., Chew, S.W.T., Lio, D.C.S., Cui, M., Liu, L., Tee, B.C.K., Xu, C., 2020. Adv. Healthc. Mater. 9, 1901683.